

Black Hole Mergers and Unstable Circular Orbits

Frans Pretorius¹ and Deepak Khurana²

¹*Department of Physics, Princeton University, Princeton, NJ 08540*

²*Indian Institute of Technology, Kharagpur*

We describe recent numerical simulations of the merger of a class of equal mass, non-spinning, eccentric binary black hole systems in general relativity. We show that with appropriate fine-tuning of the initial conditions to a region of parameter space we denote the *threshold of immediate merger*, the binary enters a phase of close interaction in a near-circular orbit, stays there for an amount of time proportional to logarithmic distance from the threshold in parameter space, then either separates or merges to form a single Kerr black hole. To gain a better understanding of this phenomena we study an analogous problem in the evolution of equatorial geodesics about a central Kerr black hole. A similar *threshold of capture* exists for appropriate classes of initial conditions, and tuning to threshold the geodesics approach one of the unstable circular geodesics of the Kerr spacetime. Remarkably, with a natural mapping of the parameters of the geodesic to that of the equal mass system, the scaling exponent describing the whirl phase of each system turns out to be quite similar. Armed with this lone piece of evidence that an approximate correspondence might exist between near-threshold evolution of geodesics and generic binary mergers, we illustrate how this information can be used to estimate the cross section and energy emitted in the ultra relativistic black hole scattering problem. This could eventually be of use in providing estimates for the related problem of parton collisions at the Large Hadron Collider in extra dimension scenarios where black holes are produced.

I. INTRODUCTION

Gravitational physics is entering an exciting era. The construction of gravitational wave detectors that are expected to be sensitive enough to observe many astrophysical phenomena where strong-field gravity plays an important role should teach us much about the cosmos and the structure of spacetime. Suggestions that we may live in a universe with more than 3 spatial dimensions [1, 2] offer the intriguing possibility that the Planck scale could be within reach of energies attainable by the Large Hadron Collider (LHC) [3, 4, 5]. This implies that the LHC may be able to probe the quantum gravity regime, and that black holes could be produced in substantial quantities by the particle collisions. Similarly, cosmic ray collisions with the earth would produce black holes [6], and this may be detected with current or near-future cosmic ray experiments [7]. Understanding the nature of black hole collisions within the theory of general relativity will be important in describing and interpreting many of these fascinating phenomena, if detected.

The past couple of years has witnessed several breakthroughs in numerical relativity[8, 9, 10], allowing for the solution of the field equations describing black hole mergers in many situations. However a vast region of interesting parameter space is unexplored, and it will be several years at least before a decent understanding of black hole collisions is achieved. In this paper we describe simulations of the merger of a class of equal mass black hole binaries on initially eccentric orbits. The orbits can be labeled with a one parameter family k loosely related to the initial tangential velocities of each black hole. We find intriguing behavior tuning k to what we call the *threshold of immediate merger* separating evolu-

tions where the black holes either merge or do not during their first close encounter. The resultant evolution becomes exponentially sensitive to the initial parameter, and the binaries exhibit a period of “whirl” type behavior similar to that seen in geodesic motion [11, 12], orbiting rapidly in a near-circular configuration. Remarkably, significant amounts of gravitational radiation ($\approx 1.0 - 1.5\%$ of the rest mass energy *per orbit*) are still being emitted in this regime. Furthermore, based on the coordinate separation¹, the binaries are orbiting within what would be the innermost stable circular geodesic of a Kerr spacetime with angular momentum equal to that of the black hole that forms in the merger case.

We show that the above behavior for equal mass binaries is analogous to evolution of similar classes of geodesics in a black hole background spacetime. Namely, if we define a one parameter family of equatorial geodesics and tune to the threshold of capture, at threshold the geodesic will approach one of the unstable circular geodesics of the background spacetime, regardless of whether the initial orbit is classified as elliptic or hyperbolic. Furthermore, if we calculate the instability (or Lyapunov) exponent of the orbits near the unstable circular orbits, we find numbers that are very similar to that observed in this fully non-linear equal mass case.

The binary black hole merger simulations described here are in the rest-mass dominated regime of the problem. The close analogy with geodesic motion allows us to speculate about what might happen in the kinetic en-

¹ comparisons between the extracted waveform and that estimated using the quadrupole formula suggests the coordinate motion of the apparent horizons is quite well adapted to describing the situation[13]

ergy dominated regime. This is relevant to the ultra-relativistic black hole scattering problem and thus might have application to the LHC if the Planck scale is below the maximum energies probed by the parton collisions. In particular, by finding the critical impact parameter and stability exponent of geodesic motion, estimating the energy and angular momentum loss while the geodesic is in the whirl phase, and providing an estimate of the energy emitted for the head-on collision case in the full problem, one can come up with an estimate of the energy emitted to gravitational waves as a function of impact parameter. We also speculate that at threshold, *all* of the kinetic energy of the system is converted to gravitational waves, which can be an arbitrarily large fraction of the total energy.

The outline of the rest of the paper is as follows. In Sec.II we summarize the numerical code; in Sec.III we describe the simulation results; in Sec.IV we describe the geodesic analog; in Sec.V we discuss all the results, speculating what must happen beyond the equal mass, non-spinning case, and how the results might carry over to the kinetic energy dominated regime and be applied to the BH scattering problem; in Sec.VI we provide some concluding remarks and a discussion of future related work. The technique we use for geodesic integration is described in the appendix.

II. OVERVIEW OF THE EQUATIONS AND SOLUTION METHOD

The Einstein Field Equations (EFE) in generalized harmonic form have been discussed in much detail elsewhere [14, 15, 16, 17, 18, 19, 20, 21, 22, 23] so for brevity here we simply list the equations and briefly mention the numerical code solving these equations.

A. formalism

We solve for a spacetime described by the line element ds with metric tensor g_{ab} and coordinates $x^a = (t, x, y, z)$ ²

$$ds^2 = g_{ab}dx^a dx^b, \quad (1)$$

using the EFE in generalized harmonic (GH) form with *constraint damping* [24, 25]:

$$\begin{aligned} & \frac{1}{2}g^{cd}g_{ab,cd} + g^{cd}{}_{(a}{}_{b)}{}_{,c} + H_{(a,b)} - H_d\Gamma_{ab}^d \\ & + \Gamma_{bd}^c\Gamma_{ac}^d + \kappa \left(n_{(a}C_{b)} - \frac{1}{2}g_{ab}n^dC_d \right) \end{aligned}$$

² We use a comma (,) to denote partial differentiation, and we use units where Newton's constant $G = 1$ and the speed of like $c = 1$

$$= -8\pi \left(T_{\alpha\beta} - \frac{1}{2}g_{\alpha\beta}T \right). \quad (2)$$

In the above, Γ_{ab}^c are the Christoffel symbols

$$\Gamma_{ab}^c = \frac{1}{2}g^{ce} [g_{ae,b} + g_{be,a} - g_{ab,e}] \quad (3)$$

T_{ab} is the stress energy tensor with trace T , H_a are the GH *source functions* defined via

$$\square x^c = H^c, \quad (4)$$

κ is a parameter multiplying the constraint damping terms, n_a a timelike vector, and C_a are the constraints:

$$C^a \equiv H^a - \square x^a. \quad (5)$$

Any solution to the Einstein equations must have $C^a = 0$; in a consistent numerical evolution the constraints will be zero to within the truncation error of the numerical scheme. For n^a we use the usual hypersurface unit normal vector $n^a = 1/\alpha(\partial/\partial t)^a$, where α is called the lapse function.

We couple in a massless scalar field Φ as the matter source, which satisfies the wave equation

$$\square\Phi = 0, \quad (6)$$

and has a stress energy tensor

$$T_{ab} = 2\Phi_{,a}\Phi_{,b} - g_{ab}\Phi_{,c}\Phi^{,c}, \quad (7)$$

The following equations are used to evolve the source functions:

$$\square H_t = -\xi_1 \frac{\alpha - 1}{\alpha^\eta} + \xi_2 H_{t,\nu} n^\nu, \quad H_i = 0. \quad (8)$$

This equation for H_t is a damped wave equation with a forcing function designed to prevent the lapse α from deviating too far from its Minkowski value of 1. The parameter ξ_2 controls the damping term, and ξ_1, η regulate the forcing term. The particular parameter values are as described in [21].

B. Boosted Scalar Field Initial Data

For initial conditions we use two boosted scalar field pulses, as described in detail in [21]. These pulses very quickly undergo gravitational collapse and form a pair of black holes in a bound orbit, with most ($\approx 85\%$) of the scalar field energy falling into the black holes, the rest radiating away on roughly the light-crossing time scale of the orbit. At the initial time we assume the corresponding spatial geometry is conformally flat and maximal, and solve the Hamiltonian and momentum constraint equations together with the maximal slicing condition for self-consistent initial conditions. For the remaining coordinate degrees of freedom we choose the spacetime slice to

be harmonic at $t = 0$.

C. Numerical code

The evolution code, described in detail in [19], uses second order accurate finite difference discretization with adaptive mesh refinement, a coordinate system compactified to spatial infinity and excision techniques to deal with the singularities inside of the black holes. Properties of the black holes are measured using apparent horizon (AH) properties, and gravitational wave information is extracted using the Newman Penrose formalism with the extraction radius placed a distance of $50m$ from the origin, where $m = m_1 + m_2$ is the total, initial AH masses of the individual black holes measured after the majority of scalar field energy has been accreted.

III. THE THRESHOLD OF “IMMEDIATE” MERGER

Here we present one of the main results of this paper, namely we give evidence that there are regions in the parameter space of the two body problem in full general relativity where the black holes evolve toward an *unstable circular orbit*, remain in that configuration for an amount of time sensitively related to the initial conditions, then either plunge toward coalescence or separate. In the case where the black holes separate after the circular motion they could possibly merge at some time in the future. These regions in parameter space can be found by examining suitable one parameter families p of initial conditions, where $p_i < p < p_s$ smoothly interpolates between an evolution with $p = p_i$ where a merger occurs promptly within $t = t_i$, and an evolution with $p = p_s$ where after some amount of time $t_s \gg t_i$ no merger has occurred. The unstable circular orbit is approached near the *threshold of immediate merger* at $p \approx p^*$, where for $p < p^*$ merger occurs promptly, while for $p > p^*$ it does not³. The number of orbits n observed near threshold is found to scale as

$$e^n \propto |p - p^*|^{-\gamma}. \quad (9)$$

Note that due to the energy loss via gravitational radiation the threshold cannot be “sharp”, i.e. if the time $t_m(p)$ to merger is plotted as a function of p , this will *not* have a discontinuous step at $p = p^*$. There will be a maximum number of orbits N for a given class of initial conditions, and what from a distance might appear like a step function will be resolved into a smooth transition over a region of size $\delta p \approx e^{-N/\gamma}$.

We cannot *prove* some of the statements made in the preceding paragraph, in particular since the full numerical simulations are so computationally expensive we have only studied one class of initial conditions in detail. However, these simulation results, the striking similarity between them and the geodesic analogue presented in the next section, and trying to understand what must happen at a generic threshold as discussed in Sec. V provides quite a compelling case for this behavior.

A. Simulation Results

Here we describe results from the evolution of a class of scalar field collapse binary (SFCB) simulations discussed before in [21]. The new simulation data presented here includes several higher resolution runs tuned closer to the threshold of immediate merger, and so now we have significantly more confidence that we are converging to this phenomena in the two body problem. Below we give a brief summary of the initial conditions, and focus on evolution results of relevance to classifying and understanding the immediate-merger-threshold scenario. More background details can be found in [21].

For initial conditions we begin with two identical boosted scalar field distributions, one located at a coordinate location of $(x, y, z) = (4.45m, 0, 0)$ and given a boost with boost parameter k in the positive- y direction, while the other is located at $(x, y, z) = (-4.45m, 0, 0)$ and given a boost k in the negative- y direction (the proper separation is initially $10.8m$). The scale m here is the sum of apparent horizon masses measured around $t = 30m$ after evolution has begun, which is after essentially all of the collapsing scalar field energy has either accreted into the newly formed black holes or is on its way to escaping to infinity. Approximately 85% of the initial scalar field energy falls into the black holes. Thus k labels our family of initial conditions. Note that k is related to though not exactly the same as the initial velocities the black holes will have. With $k = 0$ we have a head-on collision, i.e. a prompt merger, while for k sufficiently large the black holes are deflected but fly apart. Thus k describes an appropriate family to study the threshold of immediate merger.

Fig. 1 shows $n(k)$ (9) for the cases that merged ($k < k^*$), while Fig. 2 shows $n(k)$ for the cases that separated after the initial whirling motion. In the former plot n is calculated as the total phase angle ϕ divided by 2π that one of the black holes moves through before a common AH is detected, while in the later case is the total ϕ evolution divided by 2π undergone by the black hole in returning to its original coordinate distance from the origin. An example of the orbital trajectories is shown in Fig. 3. Fig. 4 shows the total energy radiated in gravitational waves from these simulations, and Fig. 5 shows a sample of the waveform from a couple of the simulations measured using both the Newman-Penrose scalar Ψ_4 and the quadrupole formula.

³ note that depending on the parameter that is being varied the magnitude of p relative to p^* denoting prompt merger can be inverted

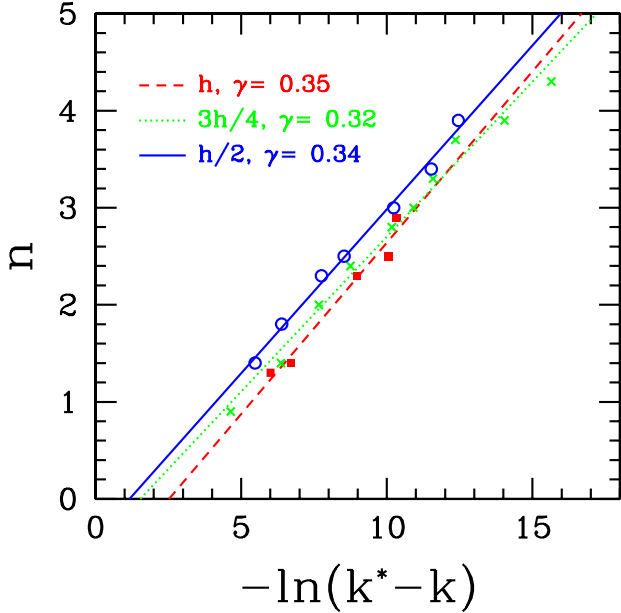


FIG. 1: The number of orbits n versus logarithmic distance of the initial boost parameter k from the immediate merger threshold k^* , for evolutions that did result in a merger. Results from the three resolutions are plotted, and a least-squares fit to each set of data assuming the relation (9).

From the data shown in Fig. 1 we estimate $\gamma = 0.35 \pm 0.03$ for this family of initial data. It is difficult to calculate the uncertainty in this quantity. In theory convergence testing should be sufficient, though here each resolution has a different number of points, so the intrinsic error in a linear regression fit will be different. Furthermore, we are assuming (9) holds, and it most certainly does not exactly. Also, since each set of simulations span a different range in $k - k^*$ this will cause some variation in the measured γ in addition to truncation and small sample size errors. We have therefore simply taken the uncertainty to be the difference in γ between the medium and higher resolution simulations (which is roughly what it would be if only truncation errors were responsible for the differences). A summary of the three characteristic resolutions used is listed in Table I.

IV. THE GEODESIC ANALOGUE

To gain insight into what is happening when tuning to the threshold of immediate merger it is useful to compare to a geodesic analogue of this behavior. Specifically, we will play the same threshold game with geodesics in a Kerr background by constructing a one parameter family p of geodesics where for $p < p^*$ the geodesics eventually fall into the black hole, while for $p > p^*$ they do not. For families of bound (elliptic) orbits, the latter subset of parameter space exhibit *zoom-whirl* behavior—the

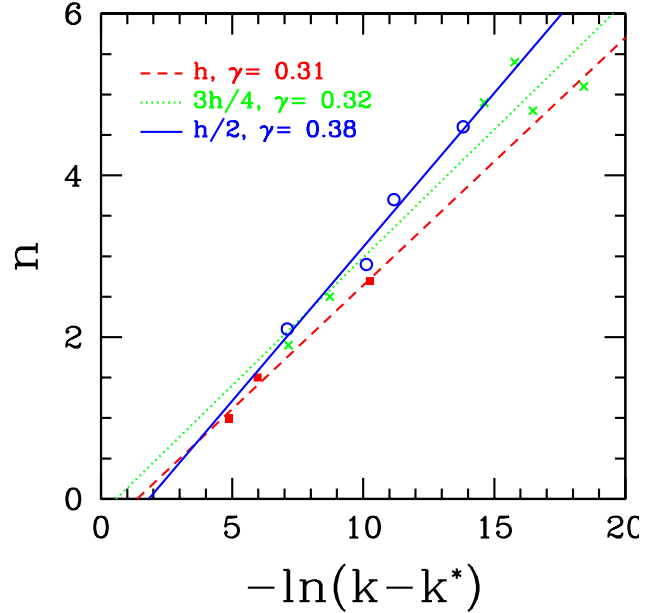


FIG. 2: Data as in Fig. 1, though here from evolutions that did *not* merge during the time of the simulation (i.e. $k > k^*$).

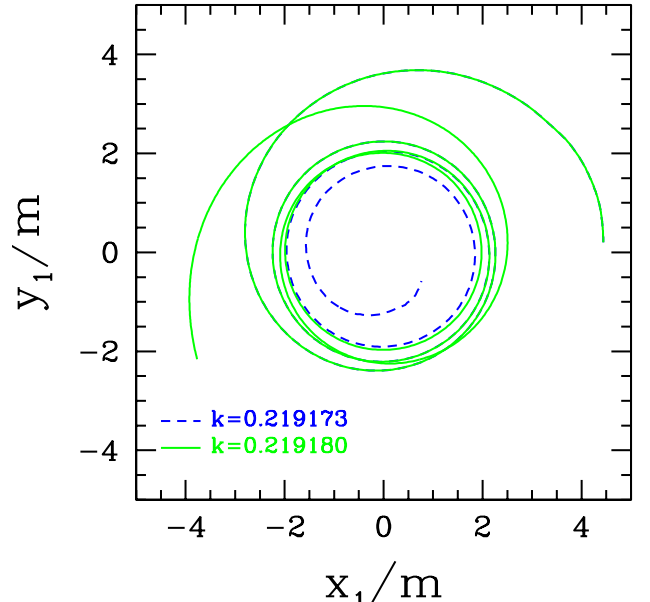


FIG. 3: Plots of the orbital motion from the two higher resolution simulations ($h/2$) tuned closest to threshold (only the coordinate motion of a single black hole—initially at positive x —is shown for clarity). The dashed curve is the case resulting in a merger, and the curve ends once a common apparent horizon is first detected, while for the solid curve the black holes separate again and here the curve ends when the simulation was stopped.

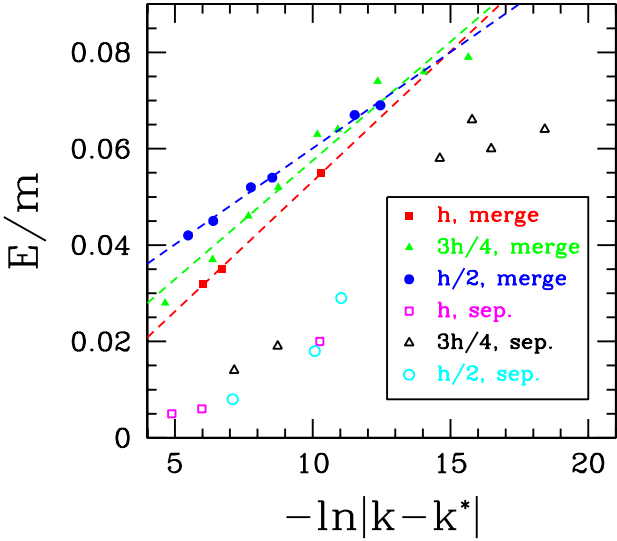


FIG. 4: The total energy radiated in gravitational waves plotted as a function of logarithmic distance from the immediate merger threshold. We have overlaid the data from both super and sub critical cases, though for clarity have only added the linear regression line for the cases that merged.

“Resolution”	wave-zone res.	orbital-zone res.	BH res.
h	$1.7M_0$	$0.23M_0$	$0.057M_0$
$3/4$ h	$1.3M_0$	$0.17M_0$	$0.043M_0$
$1/2$ h	$0.85M_0$	$0.12M_0$	$0.029M_0$

TABLE I: The three sets of characteristic resolutions used in simulation results presented here, were each resolution is labeled relative to the coarsest resolution h . The grid is adaptive with a total of 8 levels of refinement, and the coordinate system is compactified. The wave zone is defined to be at $r = 50M_0$, the orbital zone within about $r = 10M_0$ and the black hole zone is within $2 - 3M_0$ of each apparent horizon. A CFL (Courant-Friedrichs-Lowy) factor of 0.15 was used in all cases.

geodesics start some distance from the central black hole, move in close to the black hole where they whirl around for several orbits, then zoom out again to the original distance; this behavior then repeats. For the case $p < p^*$ the initial behavior is similar, namely the geodesic moves in from a distance and starts whirling about the black hole, but then plunges into the black hole. The number of whirl orbits increases as p approaches p^* , going to infinity in the limit. In this limit, the whirl part of the orbit comes arbitrarily close to one of the unstable circular geodesics of the spacetime (we are restricting attention to equatorial orbits here). Qualitatively the same behavior is seen in families of unbound (hyperbolic) geodesics, the only difference is that there is only one episode of whirling before the subset of geodesics that do not fall into the black hole escape to infinity.

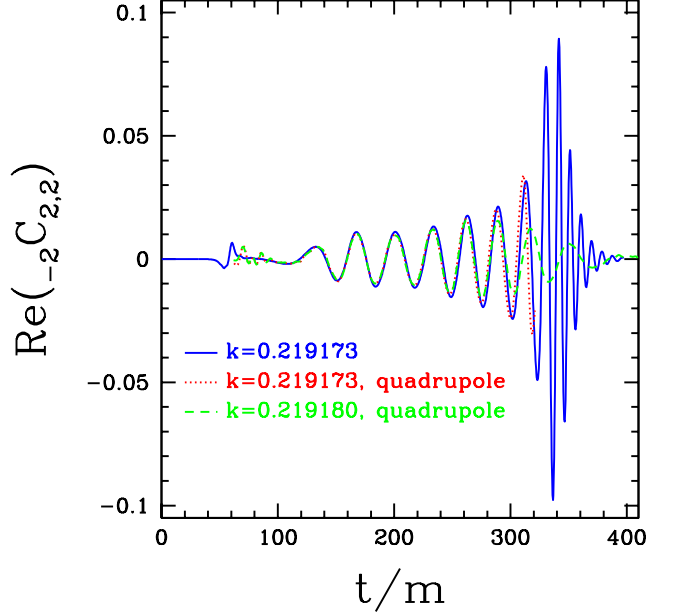


FIG. 5: The gravitational waves emitted during a merger event. Here we show the real part of the dominant spin weight -2 , $\ell = 2$, $m = 2$ spherical harmonic component of Ψ_4 . The solid curve is the merger case tuned closest to threshold (from the higher resolution simulations). The dotted curve was computed by taking the coordinate motion of the AH’s from this simulation (see Fig.3), assuming they represent the locations of point particles of mass $m/2$, and plugging the result into the quadrupole formula; this waveform ends once a common horizon is formed. The dashed curve shows the same information as the dotted curve, but here the data is from the non-merger case tuned closest to threshold. Note that the two curves from the quadrupole formula were shifted in time to account for the propagation time to the sphere at $r = 50m$ where Ψ_4 was measured.

This behavior is not only qualitatively similar to what is observed in the full merger simulations, there is also quantitative similarity comparing the scaling exponent γ in (9). Note that there even *is* a geodesic analogue is surprising, in particular if we take what the analogue is telling us at face value: in this fine tuned regime the binaries are approaching an *unstable circular* orbit. In the full problem, one might guess that even if the binaries do temporarily approach what is an unstable circular orbit, then surely the “perturbation” implied by the rather strong gravitational wave emission with this close separation would quickly force a merger? However this does not seem to happen, and moreover we speculate that with sufficiently fine-tuned initial conditions the binary can remain in this regime until close to as much energy as is theoretically possible is radiated away in gravitational waves (more on this in Sec.V).

In the remainder of this section we describe the geodesic analogue in detail, first giving an analytical calculation of the scaling exponent γ in Sec.IV A, then show-

ing results from numerical integration in Sec.IV B.

A. Calculating γ from perturbation theory

Here we calculate γ by finding the instability exponent λ of unstable circular geodesics. Our analysis mirrors the technique and formalism of [26] for Schwarzschild space-time; here we extend the result to equatorial orbits of Kerr. We will perform the calculation in Boyer-Lindquist coordinates, in which the Kerr metric takes the following form

$$ds^2 = - \left(1 - \frac{2mr}{\Sigma}\right) dt^2 + \frac{\Sigma}{\Delta} dr^2 + \Sigma d\theta^2 + R^2 \sin^2 \theta d\phi^2 - \frac{4mar \sin^2 \theta}{\Sigma} d\phi dt, \quad (10)$$

where

$$\Sigma = r^2 + a^2 \cos^2 \theta, \quad (11)$$

$$R^2 = r^2 + a^2 + \frac{2ma^2 r \sin^2 \theta}{\Sigma}, \quad (12)$$

$$\Delta = r^2 + a^2 - 2mr. \quad (13)$$

m is the total mass of the black hole, and $J = am$ the total angular momentum.

First, we want to relate λ , the growth rate of radial perturbations of the orbits in coordinate time t , to γ , that characterizes how the number of orbits increase as the logarithmic distance to the critical parameter decreases. The orbital angular frequency is

$$\omega = \dot{\phi}, \quad (14)$$

where the overdot (\cdot) denotes d/dt . We will start with a geodesic with initial conditions $r(t=0) = r_0 + \delta r_0$, where r_0 is the radial coordinate of one of the unstable circular orbits, and δr_0 is a small perturbation. To linear order the growth of the perturbation $\delta r(t) \equiv r - r_0$ is given by

$$\delta r(t) = \delta r_0 e^{\lambda t}. \quad (15)$$

Taking the absolute value and then natural logarithm of both sides we get

$$\ln |\delta r(t)| = \ln |\delta r_0| + \lambda t. \quad (16)$$

Perturbation theory breaks down when $\delta r(t) \approx 1$, which is also the time when the geodesic will either leave the vicinity of the black hole, or fall into it. By this time the number of orbits that have been complete is $n = \omega t / 2\pi$. Finally, we note that δr_0 will be proportional to $p - p^*$ for a family of geodesics that approach this unstable orbit when $p = p^*$. Substituting all this into (16) and solving for n gives

$$n = -\ln |p - p^*| \frac{\omega}{2\pi\lambda} + \text{const.}, \quad (17)$$

from which we can read off γ (9):

$$\gamma = \frac{\omega}{2\pi\lambda}. \quad (18)$$

Now we turn to the calculation of γ . We restrict attention to equatorial ($\theta = \pi/2$) geodesics, for which the corresponding Lagrangian is

$$2\mathcal{L} = - \left(1 - \frac{2m}{r}\right) t'^2 + \frac{r^2}{\Delta} r'^2 + R_0^2 \phi'^2 - \frac{4ma}{r} \phi' t', \quad (19)$$

where $R_0^2 = r^2 + a^2(1 + 2m/r)$, and the prime ($'$) denotes differentiation with respect to affine parameter s . The momentum p_q conjugate to geodesic coordinate q is $\delta\mathcal{L}/\delta q'$, and in terms of p_q and q the Euler-Lagrange equations for each pair (p_q, q) is

$$\frac{dp_q}{ds} - \frac{\delta\mathcal{L}}{\delta q} = 0 \quad (20)$$

Given that \mathcal{L} does not explicitly depend on t and ϕ we immediately obtain the following two first integrals of motion, which as usual we identify as the energy E and angular momentum L of the geodesics:

$$E \equiv -p_t = \left(1 - \frac{2m}{r}\right) t' + \frac{2ma}{r} \phi', \quad (21)$$

$$L \equiv p_\phi = R_0^2 \phi' - \frac{2ma}{r} t'. \quad (22)$$

A third constant of motion comes from the normalization condition for timelike geodesics

$$-\left(1 - \frac{2m}{r}\right) t'^2 + \frac{r^2}{\Delta} r'^2 + R_0^2 \phi'^2 - \frac{4ma}{r} \phi' t' = -1. \quad (23)$$

In principle we can use the above three equations to find a first order differential equation for $r(s)$, though instead we will follow [26] and evolve the pair (r, p_r) using (20). We shall also explore the dynamics in terms of coordinate time t rather than affine parameter s ; the transformation between them can be obtained from (21,22):

$$t' = \frac{1}{\Delta} (ER_0^2 - 2maL/r) \quad (24)$$

The resultant system of equations is

$$\dot{r} = \frac{\Delta p_r}{r^2 t'} \quad (25)$$

$$\begin{aligned} \dot{p}_r &= \frac{t'}{r^2} [\omega^2 (r^3 - ma^2) + m(2\omega - 1)] \\ &+ \frac{p_r^2}{t' r^3} [a^2 - mr] \end{aligned} \quad (26)$$

Following [26], we write the above as

$$\frac{dX_i(t)}{dt} = H_i(X_j), \quad (27)$$

where $X_i(t) = (r(t), p_r(t))$ and $H_i(X_j)$ are the right hand sides of the corresponding equations. We linearize the equations about circular orbits, namely let $X_i(t) = X_{i0} + \delta X_i(t)$ where $X_{i0} = (r = r_0, p_r = 0)$, and only keep terms linear in $\delta X_i(t)$:

$$\frac{d\delta X_i(t)}{dt} = K_{ij}\delta X_j(t), \quad (28)$$

where

$$K_{ij} = \frac{\partial H_i(X_j)}{\partial X_j} \Big|_{X_i=X_{i0}}. \quad (29)$$

The quantity λ that we are interested in is the positive real eigenvalue of (29), which exists for the range of r_0 corresponding to unstable circular orbits. We can then substitute this into (18) to find γ . After a tedious but straight-forward calculation we get

$$\gamma = \frac{r^2}{2\pi} \left[3r^2\Delta + \frac{4m}{\omega^2} (rR_0^2\omega^2 - 4m\omega r + 2m) \right]^{-1/2}, \quad (30)$$

where the above is evaluated on the given circular orbit $r = r_0$, for which (from (26))

$$\omega = \frac{m}{ma \pm \sqrt{mr^3}}. \quad (31)$$

The $+$ sign in the above corresponds to co-rotating, the $-$ sign to counter-rotating geodesics. Note that the preceding calculation is gauge dependent, though the final result (30,31) only directly refers to the radial coordinate r , and indirectly to the azimuthal coordinate ϕ in that we measure the number of orbits n completed by the geodesic. Given the axisymmetry of the spacetime we can unambiguously define n , and if desired we could re-express the equation in terms of a radius defined via the proper circumference of the geodesic (i.e. $2\pi R_0$). Though since we want to compare this to full numerical simulations where it is impossible to precisely define a value of r or spin parameter a that best mimics the geodesic problem, the difference between r and R_0 is not significant.

B. Equatorial geodesic orbits in Kerr

In the preceding section we calculated γ by examining the growth of a perturbation of an unstable circular geodesic. However, it might not be obvious that one parameter families of geodesics that smoothly interpolate between capture and non-capture will approach one of these unstable orbits as the limiting case between capture and non-capture. Here we show a few examples that this is indeed the generic behavior at threshold for equatorial geodesic families, though the *particular* unstable circular orbit that is approached depends on the initial conditions.

Fig.'s 6 and 7 show a couple of examples for two fine-tuned families of initial data in Schwarzschild spacetime ($a = 0$), integrated using the method explained in Appendix A (and note that we have integrated the geodesics in Cartesian coordinates in the Kerr-Schild form of the metric, which is horizon penetrating). Fig. 6 is an example of a hyperbolic family of orbits, Fig. 7 an elliptic family. This again illustrates that no special care need be taken in choosing a class of orbits to exhibit this behavior, merely that the orbits can be labeled by a parameter that smoothly intersects the threshold of capture. Fig. 8 shows γ as a function of r_0 , the radius of the geodesic in the whirl-phase, for a range of values of the spin parameter a . The lines in the figure were calculated using (30), and for three representative cases of a we overlay the results from a numerical calculation based on the same method used to calculate γ for the fully non-linear problem described in Sec.III. Note that each point from the numerical calculation represents fine-tuning a family of geodesics to the threshold of capture, and we typically tuned the initial conditions to within 1 part in 10^{12} (being geodesic integration on a fixed background this is a “cheap” problem). It was also not difficult to find sets of one parameter families that at threshold spanned most of the range of unstable circular orbits. For example, repeating the exact numerical setup of the binary black hole problem, we can choose the geodesic to have some initial coordinate $(x, y, z) = (d, 0, 0)$ and an initial velocity $(0, v_y, 0)$. Keeping d fixed and tuning v_y to threshold we approach an unstable circular orbit the radius of which depends on d . So repeating this threshold search for a range of d we can map out most of the range of unstable circular orbits.

On Fig. 8 we also plot an ellipse representing γ and r_0 measured in the equal mass problem described in Sec.III; the size of the ellipse depicts the numerical uncertainty in this “point”. For r_0 we have used the coordinate separation between the black holes, which, based on how well this quantity reproduces the gravitational waves emitted when plugged into the quadrupole formula (see Fig.5) suggests this is a reasonable distance indicator not subject to severe gauge artifacts⁴. The region of the diagram where γ and r_0 from the binary merger simulations fall lends support to the idea that the geodesic analogue *is* describing what is happening in the full problem—the co-rotating geodesic orbit with the same value of (r_0, γ) as the non-linear problem gives a spin parameter of ≈ 0.5 , which is close to that of the final merged black hole of ≈ 0.7 .

⁴ Another suggestion might be to use the proper distance between the two horizons; however this, when used in the quadrupole formula, overestimates the energy by almost a factor of 2.

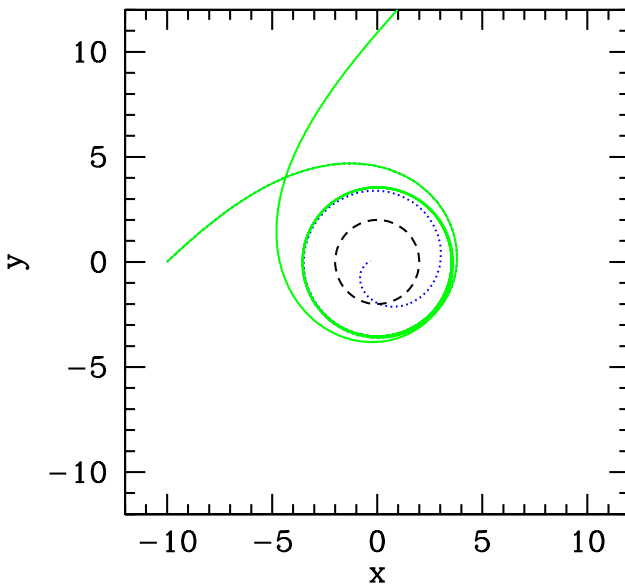


FIG. 6: Plots of two timelike geodesics of Schwarzschild ($m = 1$) spacetime tuned close to the threshold of capture. The geodesic integration was started at $(x, y, z) = (-10, 0, 0)$, the geodesics given a velocity of v , and the parameter used to find the threshold was the initial angle θ of the tangent vector relative to the x-axis. Here, the two geodesics evolve toward an unstable circular orbit at 3.54, remain close to it for roughly 6 orbits, then the one with $\theta < \theta^*$ (dotted curve) falls into the black hole while the other (solid curve) escapes. The dashed circle is the location of the event horizon. Note that the unstable circular orbit that is approached has $r < 4$, which is consistent with the orbit being unbound.

V. DISCUSSION

In Sec.III we gave evidence of a “threshold of immediate merger” in the binary black hole problem for one parameter families of initial data that interpolate smoothly between a scenario of prompt merger at one extreme and non-merger (or merger much further into the future) at the other extreme. Near threshold evolutions were marked by a period of near-circular orbital evolution at very close separation, significant gravitational wave emission, and exponential sensitivity to initial conditions. In Sec.IV we demonstrated that this behavior was quantitatively similar to equatorial geodesic behavior in a Kerr background, where the corresponding threshold is that of capture of the geodesic. Without the geodesic analogue this behavior in the full problem might seem very bizarre, and indeed even with the geodesic analogy it is still rather surprising. For given how unstable the circular orbits are that are approached at threshold, one would imagine that a “perturbation” such as the emission of a significant amount of gravitational radiation per orbit would make such an orbit unattainable away from the geodesic approximation. However, as we will try to argue

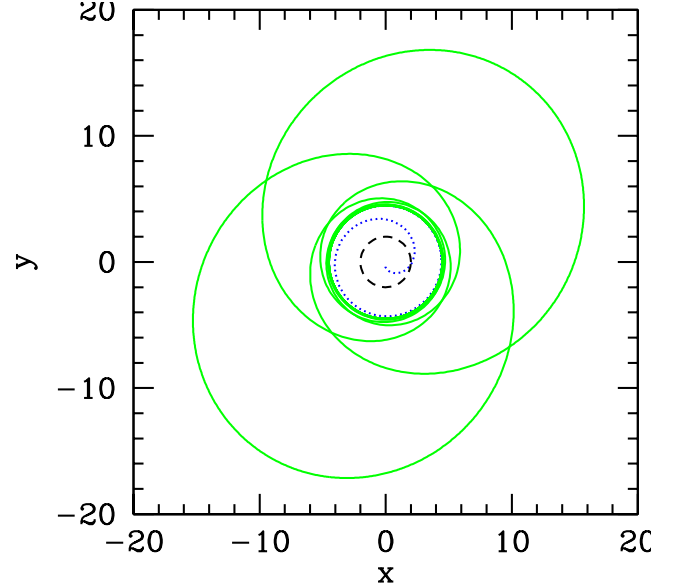


FIG. 7: A second example of timelike geodesics of Schwarzschild ($m = 1$) spacetime tuned close to the threshold of capture. Here, the geodesic integration was started at $(x, y, z) = (-4.5, 0, 0)$, and the parameter tuned to threshold was the initial velocity $v = (0, v_y, 0)$ in the y direction. In other words, we are effectively starting on an unstable circular orbit with a “perturbation” $v_y - v_y^*$. The two geodesic orbits shown here remain close to $r = 4.5$ for about 8 orbits, one (dotted curve) then falls into the black hole, while the other escapes. Since $r > 4$ this is a bound orbit, and the geodesic “zooms” out to some distance before returning to $r \approx 4.5$ to undergo another “whirl” episode. Here we show two full zoom-whirl episodes (and note that this is *not* a closed orbit; the integration was stopped during the start of the third whirl phase).

in Sec.V A below, this behavior is almost “obvious” if we try to imagine the possible orbits that could arise in the full problem. The argument applies to the generic scenario of unequal mass, arbitrary spin initial conditions, however the argument cannot claim that generically there will be any relationship with unstable geodesics of black hole spacetimes. Near-threshold orbits almost certainly do *not* have astrophysical significance due to the fine-tuning required to reach them, however if large extra dimensions exists and will result in significant black hole production at the LHC, this behavior could have some application there—we discuss this in Sec. V B.

A. Beyond equal mass non-spinning mergers

Consider a smooth one-parameter family b of initial conditions for two black holes of arbitrary masses and spins that straddle a regime of immediate merger. We further assume that the parameter is monotonic in that the threshold is only crossed once as b is varied (this also

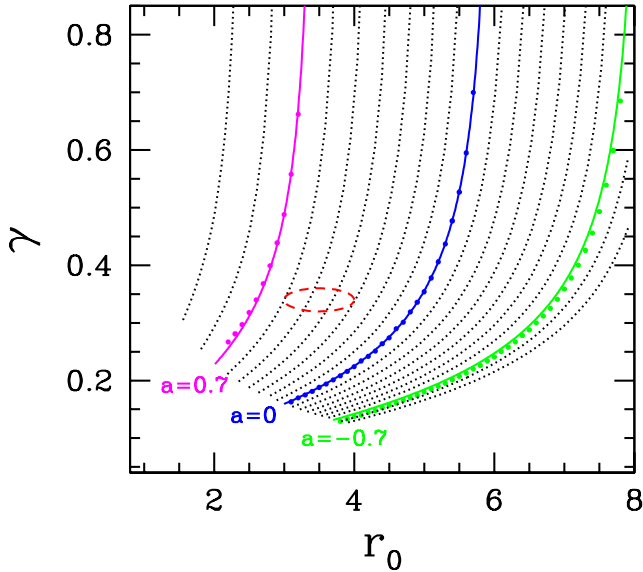


FIG. 8: Plots of $\gamma(r_0)$ for Kerr equatorial geodesics (30), for values of the spin parameter a ranging from $a = -0.9$ (right-most curve) to $a = 0.9$ (left-most curve) with intervals of 0.1. For three values of a ($0, \pm 0.7$) we plot $\gamma(r_0)$ calculated using geodesic integration tuning to the threshold of immediate capture. Specifically, *each point* depicted in the figure shows results of a bisection search to the threshold of capture for a one parameter family of geodesics; the value of r_0 is extracted from the nearest-to-threshold solution, and γ is obtained from data similar to that shown in Fig.1. The dashed ellipse shown in the figure is the value of γ (enlarged from a point to include estimated uncertainties) extracted from the fully non-linear evolutions described in Sec.III. This is in rather remarkable agreement with the geodesic results given that the final spin of the black hole is 0.68 ± 0.05 , and the trend from the simulations shows r_0 is slowly decreasing as one approaches the threshold, suggesting that the ellipse would shift to the left if we could tune closer to threshold. The near-critical geodesics at the center of the dashed ellipse have an eccentricity of $e \approx 0.5$, which might be one way to define what the effective initial eccentricity of the equal mass system is.

assumes that the threshold is not fractal in nature). Let $b = b_1$ denote one extreme (merger), $b = b_2$ the other (deflection). Now choose a value of b halfway between these two: $b_3 = (b_1 + b_2)/2$. By the assumed smoothness and monotonicity of b the resultant orbit must lie *between* the first two orbits⁵, and given that one orbit is anchored in a merged black hole, the black holes in the new orbit must spend more time in close proximity than either of the preceding cases before merging or separating—this is illustrated in Fig. 9. Continuing the

bisection therefore forces the corresponding binary system to approach an every lengthier whirl-like period of evolution. However, since more time is spent in a tight orbit, more energy will be radiated, and if the binary was initially unbound, after a certain amount of fine-tuning the system will become bound. Continuing the process beyond this point (or from initial conditions that were bound to begin with), the effective apoaps of the orbit for the cases that separate must decrease as the threshold is approached. Gravitational radiation therefore puts a limit to this process, ending it once enough energy has been radiated so that the next apoaps decreases to the radius of the orbit the binary is on during the whirl phase. Of course, approaching this point the notion of an “immediate merger” will fade, for ever sooner after separating the binaries will merge.

The preceding argument appeals to continuity of the orbital trajectories as a function of a smooth initial data parameter b . One way of preserving continuity, yet having the whirl regime terminate before all possible energy has been radiated, is if at some distance from threshold the encompassing black hole forms while the two black holes were still in the whirl phase. However, given that both the simulations shown in Sec.III and the geodesics in Sec.IV have a distinct plunge phase for the cases that do merge, we think this possibility is unlikely. One interesting question then is how much binding energy could be extracted at threshold via gravitational waves. If cosmic censorship holds then an upper limit is given by Hawking’s area theorem. The exact amount depends on the angular momentum of the final black hole; if it is non-rotating a maximum of 29% of the rest mass could be radiated; for the case studied here if the trend continues and the final spin remains $a \approx 0.7$, 24% could be radiated. It is interesting that cosmic censorship imposes such a limit in the binary merger process, for when slowly lowering a small mass to a black hole it is theoretically possible to extract all of the rest mass energy of the object before it falls through the horizon. In the high-speed scattering problem where the kinetic energy of the black holes dominate the net energy, if the argument outlined in the previous paragraph holds then it should be possible for *all* the *kinetic* energy of the system to be emitted as gravitational waves at threshold. This can be an arbitrarily large fraction of the total energy of the system.

We note that for the above arguments to be valid it is *crucial* that two distinct end-states exist in the scattering problem. In Newtonian gravity for two point masses, for example, this type of behavior cannot exist because there is no merger end-state. It is also interesting that in the geodesic problem the whirl-type behavior that arises at threshold is intimately connected to the existence of unstable circular orbits; this makes it tempting to think that there may be some deep connection between the existence of unstable geodesics in Kerr and the fact that black holes *merge* when they collide in general relativity.

⁵ though with spins the orbital plane will precess, making the trajectories curves in 3D space and preventing a simple and precise notion of “between”

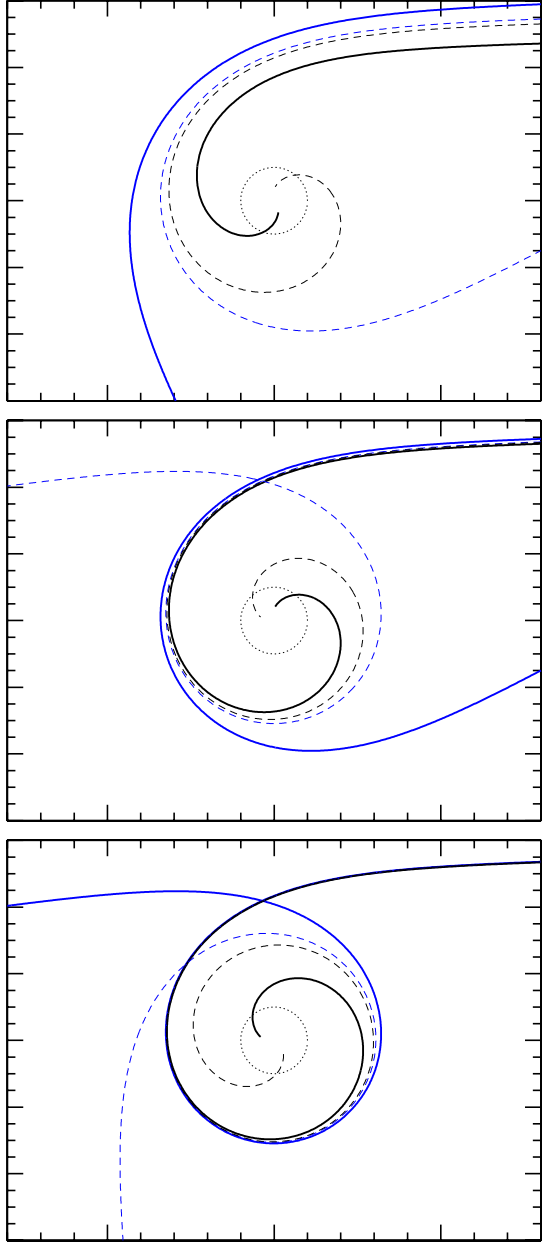


FIG. 9: A schematic illustration of why an immediate threshold must exist for the generic scattering problem. Each panel shows several hypothetical trajectories of one black hole in a two body interaction in the center of mass frame; for clarity the second black hole is not shown (in terms of the coordinates (x_1, y_1) of the first black hole with mass m_1 the second black hole of mass m_2 would have coordinates $(x_2, y_2) = -m_1/m_2(x_1, y_1)$). The two thicker solid curves represent impact parameters bracketing the threshold, i.e. in one case there is a merger, in the other a deflection. The two thinner dashed curves represent the two possible trajectories for an impact parameter between the bracketing cases. Going from the top to bottom panel we are successively tuning closer to threshold. It is difficult to imagine how a bisecting trajectory could *not* follow a path *between* the two bracketing trajectories as illustrated, and so tuning to threshold one forces the binaries into a close “whirling” configuration.

B. Black hole scattering at the LHC

One interesting application of this apparent analogy between the threshold of capture of geodesics and the threshold of immediate merger in the full problem is to obtain some understanding of the black hole scattering problem. This is of interest in the search for black holes that might be formed at the LHC (for a couple of review articles see [7, 27]). Consider the scattering of two black holes colliding with an impact parameter b . We would like to know $E_r(b)$, the energy radiated as a function of the impact parameter b , and the threshold impact parameter b^* below which a merger results (this would correspond to the threshold of black hole production in a particle collision of sufficiently high energy where the classical general relativistic description of the event holds). Below we illustrate how to find an approximation to $E_r(b)$ in the 4 dimensional case; certainly to be of relevance to the LHC this calculation will need to be carried out in higher dimensions, and many of the approximations made could be improved upon, though here we are more interested in presenting the main ideas.

For concreteness we consider the interaction of two equal mass, non spinning black holes of total rest mass m traveling with large center-of-mass speeds v . In this regime the total energy of the system $E = \Gamma m \equiv m/\sqrt{1-v^2}$ is dominated by the kinetic energy of the black holes. Also, for sufficiently large Γ any spins or electric charges of the black holes will become irrelevant, and so the non-spinning, uncharged case will be a good approximation to the generic high energy scattering problem⁶. Denote the threshold of immediate merger by $b = b^*$. Guided by the results presented in earlier sections, we will assume the following key pieces of information to obtain an approximation to $E_r(b)$:

- evolutions near the threshold of immediate merger b^* are characterized by the scaling relation (9): $e^n \propto |b - b^*|^\gamma$
- the critical impact parameter b^* and the scaling exponent γ can be found by considering the analogous problem of geodesic scattering in a Kerr background. The ADM mass of the background space time is E (which sets the scale for b), and has a spin parameter a equal to that of the black hole that forms in the full problem for b slightly less than b^* .
- during the whirl phase, a constant fraction ϵ of the remaining energy $E - E_r(t)$ of the system is radiated per orbit

⁶ though at energies probed by the LHC, and given that current experiments suggest the Planck scale cannot be very far below maximum LHC energies, the effects of spin and charge would be important to consider[28]

There are a couple of additional bits of information that will be needed to complete the calculation—the energy $E_{r0} \equiv E_r(0)$ emitted in a head-on collision, the value of a for the background Kerr spacetime, and the fraction ϵ of energy radiated per orbit. We will use an existing estimate of E_{r0} from the literature, argue below that a slightly less than extremal ($a = 1$) is the relevant parameter in the large Γ limit, and use the quadrupole formula for ϵ . Using the quadrupole formula together with geodesic motion is similar in spirit to the “semirelativistic approximation” used to compute waveforms for extreme mass ratio inspiral [29, 30].

To simplify the calculation we will use a normalized energy $\bar{E}_r \equiv E_r/E$, and define the following normalized impact parameter:

$$\bar{b} \equiv \frac{b}{b^*}, \quad 0 \leq b \leq b^* \quad (32)$$

$$\bar{b} \equiv \frac{b + b_c - 2b^*}{b_c - b^*}, \quad b^* \leq b \leq b_c. \quad (33)$$

b_c is a cut-off value for the impact parameter beyond which (9) ceases to offer a good approximation to the scattering behavior; geodesic integrations suggest $b_c \approx 2b^*$ in most cases. With the above normalization $0 \leq \bar{b} \leq 2$, and (9) becomes

$$n(\bar{b}) = -\gamma \ln |1 - \bar{b}|. \quad (34)$$

In the above we have added the additional approximation that $n(\bar{b} = 2) = 0$; strictly speaking n is only zero at $\bar{b} = 0$ (for non-spinning black holes) and in the limit as $\bar{b} \rightarrow \infty$. We assume that the energy \bar{E}_r emitted during the process is simply a function of \bar{b} , and hence n by the above relation

$$d\bar{E}_r/d\bar{b} = \frac{d\bar{E}_r}{dn} \frac{dn}{d\bar{b}}, \quad (35)$$

and that a constant fraction ϵ of the remaining energy is emitted per orbit in the whirl phase:

$$d\bar{E}_r/dn = \epsilon(1 - \bar{E}_r) \quad (36)$$

Integrating (35) with (34,36) then gives

$$\begin{aligned} \bar{E}_r(\bar{b}) &= 1 - (1 - \bar{E}_{r0}) (1 - \bar{b})^{\epsilon\gamma}, \quad 0 \leq \bar{b} \leq 1 \\ \bar{E}_r(\bar{b}) &= 1 - (\bar{b} - 1)^{\epsilon\gamma}, \quad 1 \leq \bar{b} \leq 2 \end{aligned} \quad (37)$$

For boundary conditions we have assumed all the energy is radiated for $\bar{b} = 1$, \bar{E}_{r0} is the energy radiated for the head-on collision case, and E drops to zero at $\bar{b} = 2$.

For interest, in the top panel of Fig.10 we show a plot of (37) with parameters plugged in from the low-speed system discussed in Sec.III. Of course, in this case $\bar{E}_r(1)$ can at most be $\approx .29$ from the area theorem, though for values of \bar{b} such that $\bar{E}_r(\bar{b}) < .29$ (37) is still valid.

Returning to the ultra-relativistic problem, we now estimate ϵ using the quadrupole formula. For a circular

orbit composed of equal mass point particles separated by a distance \bar{r} and orbiting with angular velocity $\bar{\omega}$, where the over-bars ($\bar{\cdot}$) denote that the quantities have been normalized to the remaining energy $1 - \bar{E}_r$ in the system, the quadrupole formula gives

$$\epsilon_{quad} = \frac{4\pi}{5} \bar{r}^4 \bar{\omega}^5. \quad (38)$$

So what values of $\bar{r}, \bar{\omega}$ and γ to use? In the ultra-relativistic geodesic scattering problem, the geodesics approach the light-ring (unstable circular *photon* geodesic) of the background spacetime at threshold. It also seems natural to guess that in this limit in the full problem the final angular momentum of the black hole will approach extremality. The initial angular momentum of the system with critical impact parameter is $J = b^* E/2$ (restoring units); thus the initial *effective Kerr parameter* of the orbit is $a_o = b^*/2$. A plot of b^* versus the background Kerr parameter a for geodesic motion is shown in Fig.11—note that in the limit $a/M \rightarrow 1$, $a_o \rightarrow 1$. To estimate how a_o changes during evolution, we again use quadrupole physics, which says $dJ/dt = \omega^{-1} dE/dt$, and define the instantaneous $a_o(t) \equiv J(t)/E(t)$. We then get

$$\frac{d(a_o/E)}{dn} = \frac{dE}{dn} \frac{1}{E} \left(\frac{1}{E\omega} - 2 \frac{J}{E^2} \right) \quad (39)$$

In the limit $a/M \rightarrow 1$, $J/E^2 \rightarrow 1$ initially, and using the Boyer-Lindquist value (31) for ω for a photon on the light-ring in the extremal case, we get $E\omega \rightarrow 1/2$. In other words, $d(a_o/E)/dn = 0$ in this limit, so at least to within the quadrupole approximation assuming an extremal Kerr background for the geodesic analog in the ultra relativistic limit is self consistent.

Though now we have a bit of a dilemma—in the extremal limit there are *no* unstable circular orbits of Kerr, and hence $\gamma \rightarrow \infty$! In a practical setting (such as the LHC) one of course will not be at the limit, though given how sensitive γ is to a approaching the limit it will be difficult to justify any crude estimates such as that outlined in the previous paragraph to decide which value of a to use to determine b^* and γ from geodesic motion. In the bottom panel of Fig.10 we therefore plot several possibilities for $\bar{E}_r(\bar{b})$ with a few values of a close to 1. We have used the limiting value of $\epsilon_{quad} \rightarrow \pi/40$, which is less sensitive to a than γ in the limit.

If Fig.10 gives a decent description of the ultra relativistic particle scattering problem, then even though the cross section for black hole production will to a good approximation be $\pi b^{*2}/4$, there can still be significant energy loss to gravitational waves for b up to almost twice b^* (or possibly even more, since recall that $\bar{E}_r(\bar{b} = 2) = 0$ was only an approximate boundary condition we imposed). $b^* \approx 2E$ in the limit, which implies an effective cross section for measurable energy loss of $4\pi E^2$. It is interesting that this number is identical to the order of magnitude estimate made by assuming the cross section is equal to πR_s^2 , where $R_s = 2E$ is the Schwarzschild ra-

dius corresponding to the initial center-of-mass energy. We finally note that a lower limit on the impact parameter resulting in black hole formation can be computed by searching for trapped surfaces at the moment the two shock waves representing the $\Gamma \rightarrow \infty$ particles collide; in [32] trapped surfaces were found for $b < \approx 1.5E$.

VI. SUMMARY AND CONCLUSIONS

In this paper we have described numerical simulations of the merger of a class of equal mass, zero initial spin, non-circular binary black hole systems in general relativity. For a one parameter (k) family of solutions interpolating between a deflection of the binaries without merger at one extreme of the parameter, and a prompt merger at the other extreme, we provided evidence that there is a notion of a threshold of immediate merger at $k \approx k^*$ during with the binary enters a tight near-circular whirl configuration before either separating or merging. The number of orbits n spent in the whirl is exponentially sensitive to the initial conditions: $e^n \propto |k - k^*|^\gamma$, where γ is approximately a constant. The area theorem together with measurements of the energy lost to gravitational waves suggests this whirl behavior could persist for as many 20-30 orbits for extremely fine tuned initial data, though we have only been able to tune to ≈ 5 orbits due to limited computational resources.

A second result of this work has been to show that similar behavior is observed in the analogous problem of the scattering of a one parameter family of equatorial geodesics off a Kerr black hole. At threshold, the geodesic approaches one of the unstable circular orbits of Kerr at a radius r_0 that depends on the particular family of geodesics. One quantitative similarity between the test particle and equal mass cases is we notice roughly the same scaling exponent γ with geodesics orbiting a black hole with spin parameter a close to that of the black hole that forms in the merger case in the full problem, and approaching an unstable orbit with radius similar to the coordinate separation of the black holes during their whirl phase. Comparison with the quadrupole formula for the emitted gravitational waves suggests the simulation coordinates are well adapted to the underlying physics.

The close analogy between threshold geodesic scattering and the one class of equal mass interactions studied here, together with an argument that such a threshold must exist for generic one parameter families of initial configurations with appropriate limiting cases, gives us some confidence in extrapolating this behavior to the kinetic energy dominated regime. This is of relevance to parton scattering in the LHC if large extra dimension scenarios describe these interactions in the TeV regime, for then high energy partons could form black holes, and the scattering process would be well approximated by the collision of two black holes. We presented a sketch of how the geodesic analogue could be used to estimate the black hole formation cross section, and energy radiated

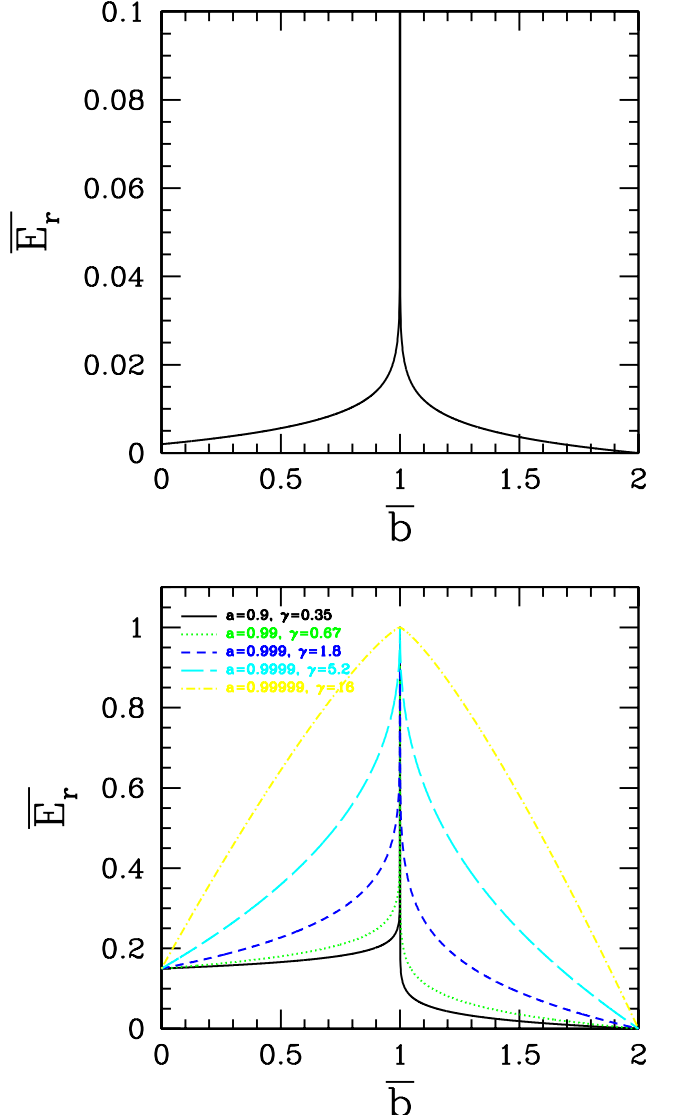


FIG. 10: Estimated fraction of the total energy radiated as a function of the impact parameter for the black hole scattering problem (37). The top panel illustrates a rest-mass dominated case, using parameters from the simulation results presented in Sec. III; here cosmic censorship would place an upper bound for $\bar{E}_r(1)$ of ≈ 0.29 . The bottom panel illustrates several curves from the kinetic energy dominated regime (note the different vertical scales in the two panels). For a concrete example we have used the value of 0.15 for \bar{E}_{r0} , which is about half that of the upper limit computed using the trapped surface method (for a review of various methods see [31]). The order-of-magnitude calculation described in the text suggests that in the ultra-relativistic limit the final state will be an extremal Kerr black hole (with negligible mass relative to the initial kinetic energy of the system). In this limit the geodesic analogue calculation becomes very sensitive to the value of the final spin parameter a , and so we show several curves for different values of a . In the limit $a \rightarrow 1$, $\gamma \rightarrow \infty$, and the estimate $\bar{E}_r(\bar{b})$ in (37) approaches a step function $\Theta(\bar{b}/2)$.

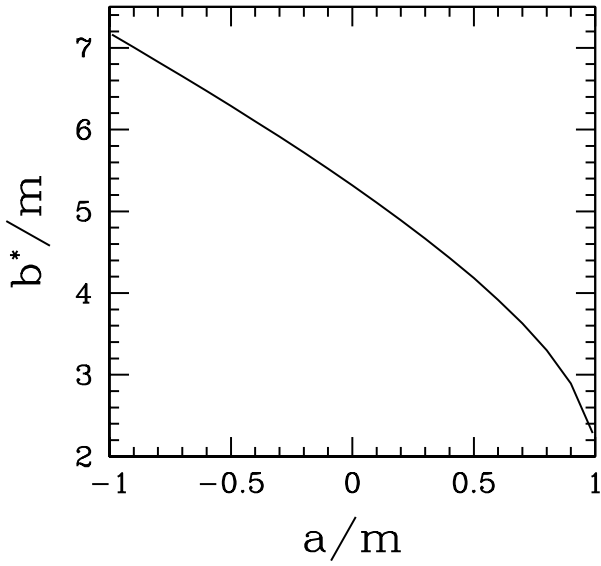


FIG. 11: The critical impact parameter b^* for equatorial geodesics with initial Lorentz $\Gamma = 10$ on a Kerr background with spin parameter a and mass m .

to gravitational waves as a function of the impact parameter. At threshold it is possible that essentially *all* the kinetic energy is radiated as gravitational waves. Away from threshold significant amounts of energy could still be radiated even if a black hole does not form.

Clearly, much of the above is pure speculation, though we believe is sufficiently interesting and relevant that it will be a fruitful endeavor to try to further establish (or disprove) the correspondence between geodesic scattering and the full problem. Simulating the ultra relativistic collision of black holes will computationally be a very challenging problem, and probably not possible to do beyond the 4-dimensional case without peta-flop scale computing. Though if the correspondence could be establish more strongly in the 4-dimensional case (which could be tackled with tera-flop resources, at least for moderately relativistic energies), then head-on collision simulations in higher dimensions together with studies of geodesic scattering and estimates of energy and angular momentum emission in gravitational waves could be used to provide useful information for the higher dimensional case.

Acknowledgments: FP would like to thank Don Page, Eric Poisson and Hirotaka Yoshino for insightful discussions. FP gratefully acknowledges research support from the CIAR, NSERC and Alberta Ingenuity. The simulations described here were performed on the University of British Columbia's **vnp4** cluster (supported by CFI and BCKDF), **WestGrid** machines (supported by CFI, ASRI and BCKDF), the Dell **Lonestar** cluster at the University of Texas in Austin, **Sharcnet** facilities (principle support by CFI, OIT and ORDCF) and the **McKenzie** cluster at CITA (supported by the CFI and

OIT).

APPENDIX A: GEODESIC INTEGRATION

In this appendix we describe the manner in which we integrate geodesics in the Kerr geometry. The original purpose of this geodesic integration method was for straight-forward incorporation into the GH evolution code, to study geodesic propagation in binary merger spacetimes. Thus the method does not take advantage of any of the symmetries of the underlying spacetime, nor uses advanced high-order ordinary differential equation (ODE) integrators. Nevertheless given the speed of contemporary desktop PC's and that geodesic integration is a one dimensional evolution there is no problem in obtaining sufficient accuracy for the purposes of the studies presented in the main sections of the paper.

Consider a spacetime with metric $g_{\alpha\beta}$

$$ds^2 = g_{\alpha\beta} dx^\alpha dx^\beta, \quad (A1)$$

and a geodesic of the spacetime described via the parametric representation of its curve $x^\alpha = x^\alpha(\lambda)$, where λ is the affine parameter along the curve. The geodesic's tangent vector is

$$u^\alpha = \frac{dx^\alpha(\lambda)}{d\lambda} \equiv x'^\alpha, \quad (A2)$$

defining prime ($'$) to denote differentiation with respect to λ . For x^α to represent a geodesic, u^α must satisfy the geodesic equation:

$$u'^\alpha + \Gamma_{\gamma\delta}^\alpha u^\gamma u^\delta = 0, \quad (A3)$$

where $\Gamma_{\gamma\delta}^\alpha$ are the Christoffel symbols (3). In terms of the coordinate position along the curve $x^\alpha(\lambda)$, (A3) can be written as:

$$x''^\alpha + \Gamma_{\gamma\delta}^\alpha x'^\gamma x'^\delta = 0. \quad (A4)$$

The causal character of the geodesic is given by the normalization of its tangent vector, as follows:

$$u^\alpha u^\beta g_{\alpha\beta} = -1 \quad \text{timelike} \quad (A5)$$

$$u^\alpha u^\beta g_{\alpha\beta} = 0 \quad \text{null} \quad (A6)$$

$$u^\alpha u^\beta g_{\alpha\beta} = 1 \quad \text{spacelike} \quad (A7)$$

We are most interested in timelike and null geodesics at the moment. For timelike geodesics, the above normalization is equivalent to demanding that λ measures the proper time of an observer moving along the geodesic. λ does not have such a straight-forward interpretation for a null geodesic; in fact, we can re-parameterize any null geodesic via a linear transformation of the form $s = a\lambda + b$, where a and b are constants.

The geodesic equations (A4) are a set of four ODEs for the coordinate position of the corresponding "particle" as

a function of affine time λ . There are at least a couple of ways to proceed to solve these equations. One is to integrate (A4) directly as a set of second order ODEs, the other is to reduce it to a system of first order ODEs. We will take the former approach as it will fit “naturally” within the generalized harmonic evolution code metrics that we want to explore the geodesic structure of. Another practical consideration in the code is that we need to integrate with respect to coordinate time t and *not* affine time λ . Define $x^0 = t$, and let x^k , $k \in 1, 2, 3$ be the three spatial coordinates, i.e. $(x^1, x^2, x^3) = (x, y, z)$. We thus want to solve for $x^k(t)$ for each geodesic. With the overdot ($\dot{\cdot}$) denoting differentiation with respect to t , using the chain rule we get:

$$\dot{x}^k = \dot{x}^k t' \quad (\text{A8})$$

$$\ddot{x}^k = \ddot{x}^k t'^2 + \dot{x}^k t'', \quad (\text{A9})$$

Substituting (A8,A9) into (A4) gives

$$\ddot{x}^\alpha t'^2 + \dot{x}^\alpha t'' + \Gamma_{\gamma\delta}^a \dot{x}^\gamma \dot{x}^\delta t'^2 = 0. \quad (\text{A10})$$

Equation (A4) for t reads:

$$t'' + \Gamma_{\gamma\delta}^0 x'^\gamma x'^\delta = 0, \quad (\text{A11})$$

and using this, with (A8) again, the geodesic equation (A10) for the spatial coordinates x^k can be written as:

$$\ddot{x}^k + (\Gamma_{\gamma\delta}^k - \dot{x}^\gamma \Gamma_{\gamma\delta}^0) \dot{x}^\gamma \dot{x}^\delta = 0. \quad (\text{A12})$$

This is the set of equations we will solve for timelike and null geodesics in a general spacetime $g_{\alpha\beta}$.

1. Initial Conditions

Since we are solving three, second order in time ODEs for each geodesic, we need *six* initial conditions per curve: the initial position $x^k(t = 0)$ and coordinate velocity $\dot{x}^k(t = 0)$ of each particle. Note that we cannot choose arbitrary velocities, as our choices must be consistent with the normalization conditions (A5,A6). There are several conceivable ways to ensure this; we will take the following route.

We begin by choosing some arbitrary direction $k^\gamma = (0, k^x, k^y, k^z)$ for the curve to point in. We need the *unit* spatial vector in this direction; call it \hat{k}^γ :

$$\hat{k}^\gamma \hat{k}^\delta g_{\gamma\delta} = 1 \quad (\text{A13})$$

and \hat{k}^γ can be found by defining

$$\hat{k}^\gamma = N k^\gamma, \quad (\text{A14})$$

plugging this into the normalization condition (A13), and solving for N . The tangent vector u^α corresponding to a

photon moving in the direction k^γ is then:

$$u^\alpha = n^\alpha + \hat{k}^\alpha \quad (\text{null case}) \quad (\text{A15})$$

For a timelike curve, in addition to the direction \hat{k}^α we can choose a velocity v (< 1). The corresponding tangent vector in this case is

$$u^\alpha = \Gamma \left(n^\alpha + v \hat{k}^\alpha \right) \quad (\text{timelike case}), \quad (\text{A16})$$

where Γ is the Lorentz gamma factor (here relative to an observer sitting at constant coordinate location and thus moving in the n^α direction):

$$\Gamma = \frac{1}{\sqrt{1 - v^2}}. \quad (\text{A17})$$

Now that we know u^α , using (A2) and (A8) we can find the initial coordinate velocities of our geodesic curves.

2. Numerical Technique

For compatibility with the metric evolution code we use a three time level scheme in a Cartesian coordinate system. The discrete version of the curve $(x(t), y(t), z(t))$ is represented by x^i, y^i, z^i , where the time $t^i = i\Delta t$, with Δt the discretization scale. Time derivatives are computed using standard second order accurate stencils:

$$\begin{aligned} \dot{f}(t)|_{t=t^i} &= \frac{f^{i+1} - f^{i-1}}{2\Delta t} + O(\Delta t^2) \\ \ddot{f}(t)|_{t=t^i} &= \frac{f^{i+1} - 2f^i + f^{i-1}}{\Delta t^2} + O(\Delta t^2). \end{aligned} \quad (\text{A18})$$

Thus, when evolving from $t = t^i$ to $t = t^{i+1}$, we require the locations of the geodesics at $t = t^i$ and $t = t^{i-1}$. In the geodesic equation (A12) the Christoffel symbols are supplied as known functions of the spacetime.

When the time differences (A18) are substituted into the geodesic equation (A12) for the time derivatives of the three coordinate positions of a geodesic, we end up with an algebraic system of three equations for three unknowns: $(x^{i+1}, y^{i+1}, z^{i+1})$. These equations are nonlinear, and so an efficient method to solve for them is via Newton iteration. We write the system of equations as

$$\mathcal{L}_j(q^k) = 0, \quad (\text{A19})$$

where $j = 1, 2, 3$ labels one of the equations, and we now use the notation q^k , $k = 1, 2, 3$ to label one of the unknowns (i.e. $q^1 = x^{i+1}, q^2 = y^{i+1}, q^3 = z^{i+1}$). Newton iteration then proceeds by writing the unknowns as a guess \hat{q}_1^k plus a correction δq^k ,

$$q^k = \hat{q}_1^k + \delta q^k, \quad (\text{A20})$$

linearizing about the guess, and solving for the correc-

tions to first order:

$$\begin{aligned}\mathcal{L}_j(q^k) &= \mathcal{L}_j(\hat{q}_1^k + \delta q^k) \\ &\approx \mathcal{L}_j|_{q^k=\hat{q}_1^k} + \frac{\partial \mathcal{L}_j}{\partial q^l}|_{q^k=\hat{q}_1^k} \cdot \delta q^l = 0.\end{aligned}\quad (\text{A21})$$

Written in terms of the residual $R_j \equiv \mathcal{L}_j(\hat{q}_1^k)$ and the Jacobian matrix $J_{jl} \equiv \frac{\partial \mathcal{L}_j}{\partial q^l}$ the resultant linear system that is solved for the correction δ_q^l is:

$$J_{jl} \cdot \delta q^l = -R_j. \quad (\text{A22})$$

After solving for the correction, the above steps are repeated with the corrected solution serving as the new guess, and the iteration proceeds until the norm of the residual is below some specified tolerance.

a. Second order accurate initial conditions

To begin evolving the geodesics at $t = 0$ with a three time level scheme, we need the initial positions x^0, y^0, z^0 at $t = 0$ and the positions x^{-1}, y^{-1}, z^{-1} at $t = -\Delta t$. One can use taylor expansions, the freely specifiable ini-

tial conditions discussed in Sec. A 1, and the geodesic equations (A12) to initialize the past time values to the necessary level of accuracy. Use the subscript 0 to refer to the analytic initial condition for a given variable; for example, for x :

$$x_0 \equiv x(t)|_{t=0}, \quad (\text{A23})$$

$$\dot{x}_0 \equiv \dot{x}(t)|_{t=0}, \quad (\text{A24})$$

$$\ddot{x}_0 \equiv \ddot{x}(t)|_{t=0}. \quad (\text{A25})$$

Then, to second order

$$x^{-1} = x_0 - \dot{x}_0 \Delta t + \ddot{x}_0 \frac{\Delta t^2}{2}. \quad (\text{A26})$$

The initial position x_0^k is freely specifiable, the initial velocity \dot{x}_0^k is calculated as described in (A1), and the geodesic equations (A12) are used to solve for \ddot{x}_0^k :

$$\ddot{x}_0^k = -(\Gamma_{\gamma\delta}^k - \dot{x}_0^k \Gamma_{\gamma\delta}^t) \dot{x}_0^\gamma \dot{x}_0^\delta. \quad (\text{A27})$$

Note the summation over all initial velocities in the above, including over $t = 1$.

[1] N. Arkani-Hamed, S. Dimopoulos and G. Dvali, “The hierarchy problem and new dimensions at a millimeter”, *Phys. Lett. B* **429**, 263 (1998)

[2] L. Randall and R. Sundrum, “Large Mass Hierarchy from a Small Extra Dimension”, *Phys. Rev. Lett.* **83**, 3370 (1999)

[3] T. Banks and W. Fischler, “A Model for High Energy Scattering in Quantum Gravity”, hep-th/9906038

[4] S.B. Giddings and S. Thomas, “High energy colliders as black hole factories: The end of short distance physics”, *Phys. Rev. D* **65**, 056010 (2002)

[5] S. Dimopoulos and G. Landsberg, “Black Holes at the Large Hadron Collider”, *Phys. Rev. Lett.* **87** 161602, (2001)

[6] J.L. Feng and A. D. Shapere, “Black hole production by cosmic rays”, *Phys. Rev. Lett.* **88** 021303, (2002)

[7] G. Landsberg, “Black Holes at Future Colliders and Beyond: a Topical Review”, *J.Phys. G***32**, R337 (2006)

[8] F. Pretorius, “Evolution of Binary Black Hole Spacetimes”, *Phys. Rev. Lett.* **95**, 121101 (2005)

[9] M. Campanelli, C.O. Lousto, P. Marronetti and Y. Zlochower, “Accurate Evolutions of Orbiting Black-Hole Binaries Without Excision”, *Phys. Rev. Lett.* **96**, 111101 (2006)

[10] J. G. Baker, J. Centrella, D. Choi, M. Koppitz and J. van Meter, “Gravitational Wave Extraction from an In-Spiraling Configuration of Merging Black Holes”, *Phys. Rev. Lett.* **96**, 111102 (2006)

[11] C. Cutler, D. Kennefick and E. Poisson, “Gravitational radiation reaction for bound motion around a Schwarzschild black hole,” *Phys. Rev. D* **50**, 3816 (1994).

[12] K. Glampedakis and D. Kennefick, “Zoom and whirl: Eccentric equatorial orbits around spinning black holes and their evolution under gravitational radiation reaction,” *Phys. Rev. D* **66**, 044002 (2002)

[13] A. Buonanno, G. Cook and F. Pretorius, “Inspiral, merger and ring-down of equal-mass black-hole binaries”, gr-qc/0610122

[14] H. Friedrich, “On the Hyperbolicity of Einstein’s and Other Gauge Field Equations”, *Commun. Math. Phys* **100**, 525 (1985)

[15] H. Friedrich, “Hyperbolic reductions for Einstein’s equations”, *Class. Quant. Grav.* **13**, 1451 (1996)

[16] D. Garfinkle, “Harmonic coordinate method for simulating generic singularities”, *Phys. Rev. D* **65**, 044029 (2002)

[17] B. Szilagyi, B. G. Schmidt and J. Winicour, “Boundary conditions in linearized harmonic gravity,” *Phys. Rev. D* **65**, 064015 (2002)

[18] B. Szilagyi and J. Winicour, “Well-Posed Initial-Boundary Evolution in General Relativity”, *Phys. Rev. D* **68**, 041501 (2003)

[19] F. Pretorius, “Numerical Relativity Using a Generalized Harmonic Decomposition”, *Class. Quant. Grav.* **22** 425, (2005)

[20] L. Lindblom, M. A. Scheel, L. E. Kidder, R. Owen and O. Rinne, “A New Generalized Harmonic Evolution System”, *Class. Quant. Grav.* **23**, S447 (2006)

[21] F. Pretorius, “Simulation of binary black hole spacetimes with a harmonic evolution scheme”, *Class. Quant. Grav.* **23**, S529 (2006)

[22] M. C. Babic, B. Szilagyi and J. Winicour, “Harmonic Initial-Boundary Evolution in General Relativity,” *Phys. Rev. D* **73**, 064017 (2006)

[23] B. Szilagyi, D. Pollney, L. Rezzolla, J. Thornburg and J. Winicour “An explicit harmonic code for black-hole evolution using excision”, gr-qc/0612150

- [24] C. Gundlach, J. M. Martin-Garcia, G. Calabrese and I. Hinder, “Constraint damping in the Z4 formulation and harmonic gauge,” *Class. Quant. Grav.* **22**, 3767 (2005).
- [25] O. Brodbeck, S. Frittelli, P. Hubner and O. A. Reula, “Einstein’s equations with asymptotically stable constraint propagation,” *J. Math. Phys.* **40**, 909 (1999)
- [26] N. Cornish and J. Levin, “Lyapunov timescales and black hole binaries”, *Class.Quant.Grav.* **20**, 1649 (2003)
- [27] D. M. Gingrich, “Black hole cross-section at the large hadron collider”, *Int.J.Mod.Phys. A***21**, 6653 (2006)
- [28] D. M. Gingrich, “Effect of charged partons on black hole production at the large hadron collider”, hep-ph/0612105
- [29] R. Ruffini and M. Sasaki, “On A Semirelativistic Treatment Of The Gravitational Radiation From A Mass Thrusted Into A Black Hole”, *Prog.Theor.Phys.* **66**, 1627 (1981)
- [30] J.R. Gair , D.J. Kennefick and S.L. Larson, “Semi-relativistic approximation to gravitational radiation from encounters with black holes”, *Phys.Rev. D***72**, 084009 (2005), *Erratum-ibid. D***74**, 109901 (2006)
- [31] V. Cardoso, E. Berti and M. Cavaglia, “What we (don’t) know about black hole formation in high-energy collisions”, *Class.Quant.Grav.* **22**, L61-R84 (2005)
- [32] H. Yoshino and Y. Nambu, “Black hole formation in the grazing collision of high-energy particles”, *Phys.Rev. D***67**, 024009 (2003)